Northumbria Research Link

ACS Energy LETTERS

LETTER

# Above 600 mV Open-Circuit Voltage BiI₃ Solar Cells

Devendra Tiwari,[†] Dominic Alibhai,[‡] and David J Fermin[*,†]

[†]School of Chemistry, University of Bristol, Bristol BS8 1TS, United Kingdom
[‡]Wolfson Bioimaging Facility, Faculty of Biomedical Sciences, University of Bristol, University Walk, Bristol BS8 1TD, United Kingdom

S *Supporting Information*

ABSTRACT: Phase-pure BiI₃ films obtained by versatile gas-phase iodination of Bi₂S₃ are investigated as an absorber in photovoltaic devices. This preparation method leads to highly crystalline BiI₃ films featuring a rhombohedral phase and a high-degree of stacking order. The films are composed of micrometer-sized flat grains distributed homogeneously across the F-doped SnO₂ (FTO) substrate, exhibiting an indirect band gap transition at 1.72 eV. High-level calculations based on G_0W_0 approximation are used to rationalize the electronic structure of BiI₃, confirming the band gap value estimated experimentally. The films show p-type conductivity with an acceptor density on the order of 10^{15} cm^{-3}. Solar cells with the architecture glass/FTO/TiO₂/BiI₃/F8/Au, where F8 is poly(9,9-di-*n*-octylfluorenyl-2,7-diyl), display a record open-circuit voltage above 600 mV and overall power conversion efficiency of 1.2% under AM 1.5G illumination. The large open-circuit potential is rationalized in terms of carrier lifetimes longer than 1 ns as probed by time-resolved photoluminescence spectroscopy.

Textured BiI₃ films — FTO/TiO₂/BiI₃/F8/Au Solar cell
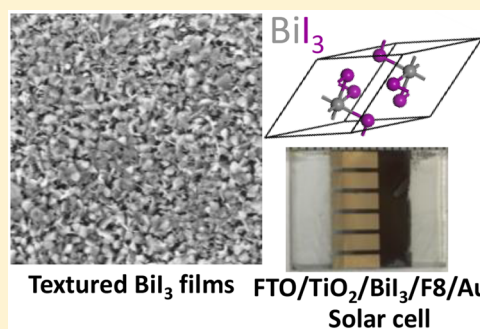
Sustainable photovoltaic (PV) technologies beyond Si solar cells represent huge opportunities in key areas such as large-scale building integration and competitive tandem technologies close to 30%.[1,2] This strategy requires new solar absorbers based on earth-abundant materials that can offer different alternatives to existing CdTe and CuInGa-(S,Se)₂ (CIGS) technologies.[3−6] Hybrid perovskite solar cells have experienced an unprecedented rise from basic science to a technology close to commercialization, particularly in the context of Si-tandem solar cells, although significant challenges remain in terms of stability.[7] Cu₂ZnSn(S,Se)₄ has been the key target in the context of earth-abundant CIGS replacement; however, efficiency remains hindered by a loss mechanism yet to be fully elucidated.[8−10] These developments have led to the establishment of guiding principles for the design of solar absorbers based on the concept of "defect-tolerant materials", with Bi being one of the elements in these strategies.[5,6] Indeed, Bi³⁺ and Pb²⁺ are heavy and highly polarizable cations associated with large spin−orbit coupling effects, dielectric constants, and band dispersion, resulting in low recombination probabilities and better charge separation.[5,6,11] Bi compounds such as methylammonium bismuth iodide, bismuth chalcohalides, bismuth sulfide, silver bismuth sulfide, and bismuth iodide have been tested as solar absorbers with power conversion efficiencies up to 6.3%.[12−19] Previously, we reported on BiFeO₃ all-oxide solar cells with a record power conversion efficiency of 4%.[18] BiI₃ is particularly attractive as a binary compound composed of low-cost elements and suitable optoelectronic properties.[20]

BiI₃ fundamental optical transitions have been reported in the range of 1.67−1.90 eV, featuring capture cross sections larger than 10^5 cm^{-1} for energies above 2 eV.[20−23] Additionally, minority carrier lifetime (τ_h) and electron mobilities (μ_e) of 1.54 ns and 250 cm^2 V^{-1} s^{-1} have been reported in BiI₃ single crystals.[20,24,25] The current record efficiency of BiI₃ thin-film cells was reported by Hamdeh and co-workers, with a V_{OC} value below 400 mV and a power conversion efficiency of approximately 1%, although no statistical analysis of these performance indicators was reported.[17] In contrast to single crystals, thin films deposited either by solution or physical vapor deposition are characterized by a shorter τ_h (250 ps), which could be a limiting factor in PV performance.[20] In this work, we develop a new methodology for preparing high-quality rhombohedral BiI₃ thin films based on gas-phase iodination of Bi₂S₃. The films exhibit a high degree stacking order with τ_h values longer than 1 ns as estimated from time-resolved photoluminescence spectroscopy. PV devices with the architecture glass/FTO/TiO₂/BiI₃/F8/Au, where F8 is poly-(9,9-di-*n*-octylfluorenyl-2,7-diyl), display a record open-circuit voltage above 600 mV and overall efficiency of 1.2% under AM
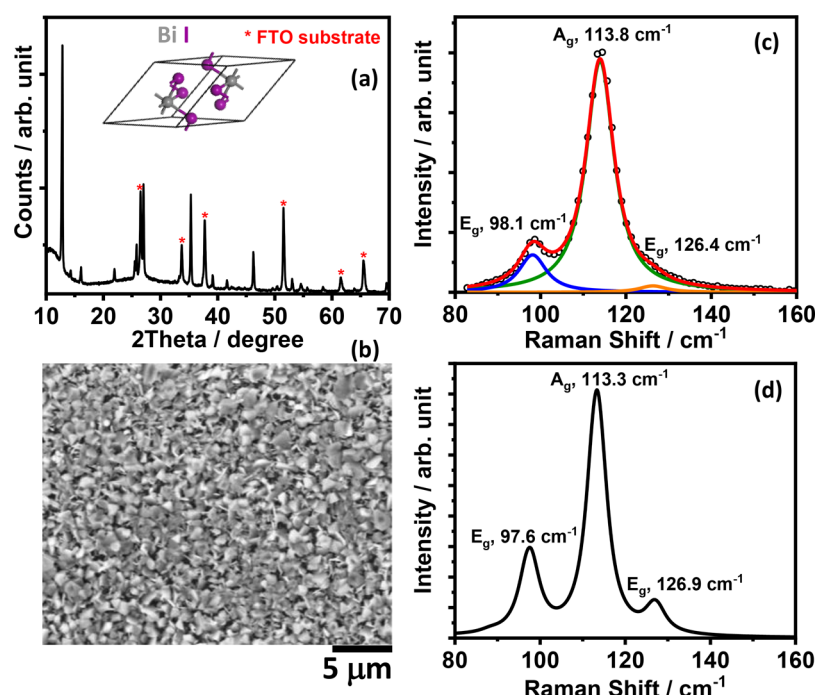
Figure 1. Structural and morphological characterization of BiI_3 thin films: XRD with the inset depicting the BiI_3 unit cell (a), top-view scanning electron micrograph (b), measured Raman spectrum under 785 nm laser excitation (c), and calculated Raman spectrum employing DFPT (d).
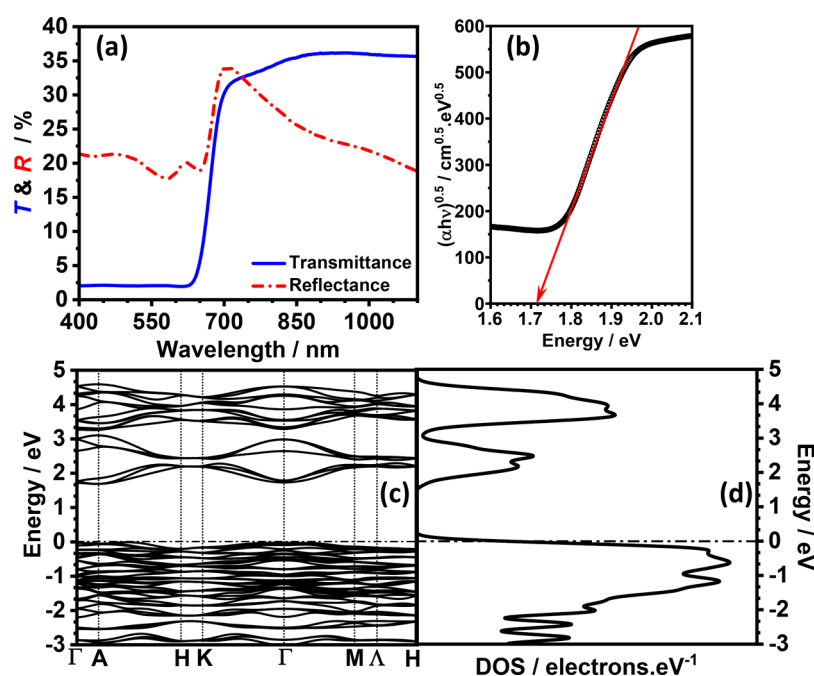

Figure 2. Transmittance and reflectance spectra of BiI_3 thin films (a), Tauc's plot showing an indirect transition at 1.72 eV (b), band structure (c), and density of states (DOS) (d) of BiI_3 calculated employing the quasiparticle G_0W_0 approximation.

1.5G illumination. Electronic and vibrational fingerprints of the phase-pure BiI_3 films are rationalized based on calculations employing G_0W_0 approximation and density functional perturbation theory (DFPT).

BiI_3 films are prepared by a sequential method starting from spin coating a $Bi(NO_3)_3$ and thiourea precursor solution onto FTO, followed by thermolysis at 200 °C to produce a homogeneous Bi_2S_3 film that is subsequently iodinated upon exposure to the I_2 gas. This methodology was inspired in our

previous report on the fabrication of PbI_2 photocathodes,[26] although in this case the Bi_2S_3 is placed above the I_2 granules, which are heated to 200 °C (see Supporting Information section S3 for further details). The reaction is governed by Pearson's hard−soft acid−base principle in which the polarizable Bi^{3+} (soft-acid) spontaneously exchanges a hard S^{2-} base partner with a polarizable I^- (soft-base).[27]

The structure, morphology, and phase purity of the as-grown BiI_3 films are investigated by X-ray diffraction (XRD) and

Raman spectroscopy (Figure 1). XRD of the film on the FTO substrate (Figure 1a) reveals crystallization of BiI$_3$ in its common rhombohedral structure ($R\bar{3}$, space group: 148). No peaks due to sulfide, oxide, and oxyiodide are detected. The high intensity of the (003) peak at ∼12° suggests a high degree of orientation along the c-axis of the unit cell. The Bi atom is octahedrally coordinated to I atoms, forming hexagonally close-packed layers interacting by a weak Van der Waals force along the c-axis with the Bi atom, effectively occupying two-thirds of the octahedral sites.[28] The SEM image in Figure 1b is characterized by flake-shaped grains with sizes in the range of 700−1200 nm homogeneously distributed across the substrate. This growth behavior is similar to that observed for PbI$_2$ films.[26]

Figure 1c displays the Raman spectrum of BiI$_3$, showing three distinctive bands assigned to A$_g$ and E$_g$ modes. These assignments are supported by theoretically calculated spectra using DFPT, as shown in Figure 1d (the full spectrum is plotted in Figure s1). The measured and calculated spectra exhibit remarkable similarity in the range of 80−160 cm^{-1}. The spectral information below 83 cm^{-1} cannot be accessed in our spectrometer. The modes at 98 and 113 cm^{-1} are LO phonon modes at the Γ and Z special points, respectively. The nature of three vibrational modes at 98, 114, and 126 cm^{-1} is captured in the movies provided in Supporting Information Movie S1 and Movie 2.

Figure 2a displays the optical transmittance and reflectance spectra of 230 nm thick BiI$_3$ films on the FTO-coated glass substrates, showing sharp absorption behavior between 650 and 700 nm. Considering an indirect band gap transition, a value of 1.72 can be estimated from the Tauc's plot in Figure 2b. As mentioned previously, there is some debate in the literature concerning the value of the indirect band gap transition, which ranges between 1.65 and 1.90 eV, with reports of direct transitions between 1.8 and 2 eV.[20−23] The dispersion in the reported experimental and computed value of E$_g$ has been found to depend on the experimental methodology and computational level.[16,20,22,23,29−33] The most detailed optical study has been reported by Podraza et al., showing an indirect transition at 1.67 eV,[22] which is close to our findings. On the other hand, the hybrid HSE functional DFT by Lehner et al. estimated a value of 1.93 eV.[16]

Figure 2c,d summarizes our estimations of the electronic structure of BiI$_3$ employing quasiparticle G$_0$W$_0$ approximation showing that the lowest-energy transition has an indirect nature with a value of 1.68 eV. Komatsu and Kaifu established that the temperature dependence of the BiI$_3$ band gap has a gradient of −3.7 × 10^{-4} eV/K between 286 and 77 K and −1.8 × 10^{-4} eV/K between 77 and 6 K.[34] On the basis of these findings, the calculated band gap is expected to decrease to approximately 1.59 eV at room temperature. It is important to highlight that G$_0$W$_0$ calculations consistently underestimated experimental band gap values by 200 meV on average in over 200 materials.[35,36] Consequently, the difference in our computed value and the experimental band gap on our thin films (Figure 2b) and on single crystals by Podraza et al.[22] can be considered within the error of the method.

Although G$_0$W$_0$ calculations provide accurate accounts of spin−orbit coupling, band dispersions, and width, this comes at the expense of high computational costs, which limit calculating the projected density of states. However, this information is available with a good level of accuracy from the elegant work by Lehner et al. employing DFT with hybrid

functionals.[16] The conduction band is formed of highly covalent I 5p and Bi 6p hybridized states split due to spin−orbit coupling, while the valence band is primarily composed of an I 5p orbital with a minor contribution from Bi 6s electrons. Calculations also show that the conduction band is much more dispersed than the valence band as a result of spin−orbit coupling promoted by the Bi^{3+} ion. This results in a lighter effective mass of electrons in comparison to holes and thus higher electron mobility. This observation is also consistent with experimental studies on BiI$_3$ single crystals, showing effective electron mass 5 times lower than that of holes and electron mobility up to 250 cm^2 V^{-1} s^{-1}.[25] The high covalent interaction in the conduction band is also responsible for a substantial in-plane Born effective charge of 5.43. These optoelectronic features are very attractive in the context of thin-film PV devices.

Electrochemical impedance spectroscopy in nonaqueous electrolyte solutions was employed to estimate the doping density of the films. Analysis based on the Mott−Schottky plot in Figure s2 confirmed the p-type nature of BiI$_3$, with estimates of the majority carrier density in the range of 2.8 × 10^{15}−1.4 × 10^{16} cm^{-3}, considering the contrast in relative permittivity between in-plane ($\varepsilon_\parallel$ = 8.6) and out-of-plane ($\varepsilon_\perp$ = 54).[37] These values should be considered as an upper limit as the effective roughness of the material is not considered in the calculations. PbI$_2$ films obtained by a similar route were also characterized by a low doping density.[26] The analysis also shows that the flat band potential (E$_{fb}$) is located at 1.53 V vs SHE, placing the valence band maxima (VBM) at approximately 5.97 eV with respect to the vacuum level, which is close to values obtained from photoemission spectroscopy.[16] Considering E$_g$ = 1.72 eV, the conduction band minima (CBM) is set close to 4.25 eV.

Current−voltage characteristics of 10 devices featuring an active area of 4 mm^2 under AM 1.5G (100 mW cm^{-2}) illumination are shown in Figure 3a. Devices were designed with an architecture glass/FTO/TiO$_2$/BiI$_3$/F8/Au, with a BiI$_3$ film thickness of 230 nm. As described in Supporting Information section S3, electron (TiO$_2$) and hole (F8) transporting layers were processed by spin-coating. The best-performing device displayed a power conversion efficiency (η) of 1.21% with a short-circuit current (J$_{SC}$), fill factor (FF), and open-circuit voltage (V$_{OC}$) of 5.28 mA/cm^2, 37.6%, and 607 mV, respectively. These figures of merit represent clear improvement over the state-of-the-art, in particular, the 200 mV increase in V$_{OC}$.[17] The external quantum efficiency (EQE) for the champion cell shows a maximum value close to 35%, as displayed in Figure 3b. The variation of the key figure of merit was less than 10%, illustrating the reproducibility in the preparation method.

The improved device performance with respect to previous reports can be linked to the device architecture and the quality of the BiI$_3$ film. Conducting polymers such as polytriarylamine (PTAA; IP = 5.1 eV) and polyindacenodithiophene-difluorobenzothiadiazole (PIDT-DFBT; IP = 5.5 eV) have been employed as hole transport layers (HTLs) by Lehner et al.[16] The HTL with a higher IP resulted in an improvement of V$_{OC}$ from 220 to 420 mV but at the cost of the short-circuit current (J$_{SC}$), leading to only an incremental change in the overall η from 0.3 to 0.32%.[16] Hamdeh et al. used a thin layer of V$_2$O$_5$, which resulted in J$_{SC}$ of up to 8 mA cm^{-2} and η of 1.0%; however, the V$_{OC}$ remained limited to 365 mV.[17] The use of F8 in our devices was inspired by Ganose et al.'s theoretical
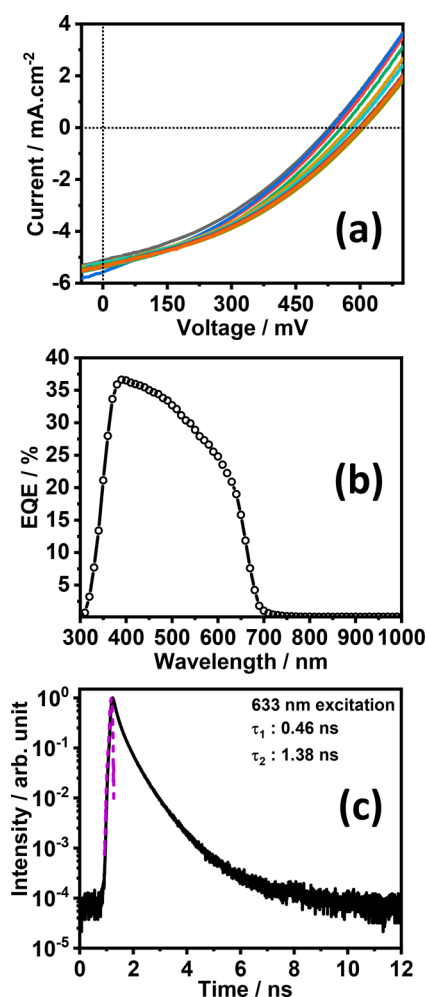
Figure 3. PV performance of glass/FTO/TiO$_2$/BiI$_3$/F8/Au devices: J–V characteristics of 10 cells under AM 1.5G (100 mW/cm^2) illumination (a) and characteristic EQE spectrum (b). Time-resolved photoluminescence spectrum of the BiI$_3$ films (c). The purple trace corresponds to the instrument response function (IRF).

studies on BiSI, suggesting that the high IP value (5.8 eV) of this polymer offers a better match to the VBM.[38] This point partially accounts for the record V_{OC} values measured in our devices. Indeed, we have investigated cells employing F8 as the HTL but following previous protocols in which commercially available BiI$_3$ powders were spin-coated to the TiO$_2$ surface (so-called "direct" method).[20] The corresponding J–V curves (Figure s3a) exhibited J_{SC} and FF values that were 10–15% lower, while the V_{OC} dropped by 56% in comparison to the devices prepared by our gas-phase iodination method. The EQE spectra also show significantly lower values at wavelengths close to the band edge for the devices prepared via the direct method (Figure s3b). These results strongly suggest that the minority carrier lifetime is significantly different in these two films.

Finally, Figure 3c shows a characteristic time-resolved photoluminescence measurement of BiI$_3$ prepared by gas-phase iodination. The data were fitted to a biexponential function, yielding two lifetime values of around 460 ps and 1.4 ns. These values are comparable to the lifetimes measured on BiI$_3$ single crystals and significantly longer than those in thin films reported in previous studies.[17,20] It is rather difficult to

quantitatively rationalize the increase in V_{OC} with carrier lifetime as there is no theoretical framework directly combining these two parameters. Repins and co-workers provided an empirical correlation after analyzing a large number of CIGS devices, showing that V_{OC} is strongly dependent on carrier lifetime in the range below 10 ns.[39] Consequently, the high quality of the BiI$_3$ thin films generated by our method is key for achieving record V_{OC} and PCE values. There is significant room for improvement in device architecture, not only in terms of better alignment of ETL and HTL layers to the absorber layer but also in the carrier collection efficiencies. Indeed, it is anticipated that interfacial recombination at the boundaries with carrier extracting layers is the main performance limiting factor in these devices.

■ ASSOCIATED CONTENT

ⓢ Supporting Information

The Supporting Information is available free of charge on the ACS Publications website at DOI: 10.1021/acsenergy-lett.8b01182.

> BiI$_3$ thin film deposition and cell fabrication, film characterization and device measurements, computational details, BiI$_3$ Raman spectrum calculated by DFPT, Mott−Schottky plot of the BiI$_3$ film in dichloromethane, and device performance of cells fabricated by direct spin-coating of BiI$_3$ particles (PDF)
>
> Movie illustrating the Raman A$_g$ vibrational mode of BiI$_3$ (AVI)
>
> Movie illustrating the Raman E$_g$ vibrational mode of BiI$_3$ (AVI)

■ AUTHOR INFORMATION

Corresponding Author

*E-mail: david.Fermin@bristol.ac.uk.

ORCID ⓘ

David J Fermin: 0000-0002-0376-5506

Notes

The authors declare no competing financial interest.
All data presented in this Letter can be freely accessed from the Bristol's Research Data Repository (https://doi.org/10.5523/bris.2b4tiz6tawpgy29o33jdjfxzk0).

■ REFERENCES

(1) Sofia, S. E.; Mailoa, J. P.; Weiss, D. N.; Stanbery, B. J.; Buonassisi, T.; Peters, I. M. Economic Viability of Thin-Film Tandem Solar Modules in the United States. *Nat. Energy* **2018**, *3*, 387−394.

(2) Ballif, C.; Lufkin, S.; Rey, E.; Perret-Aebi, L.-E. Integrated Thinking for Photovoltaics in Buildings. *Nat. Energy* **2018**, *3*, 438−442.

(3) Haegel, N. M.; Margolis, R.; Buonassisi, T.; Feldman, D.; Froitzheim, A.; Garabedian, R.; Green, M.; Glunz, S.; Henning, H. M.; Holder, B.; et al. Terawatt-Scale Photovoltaics: Trajectories and Challenges. *Science* **2017**, *356*, 141−143.

(4) Peter, L. M. Towards Sustainable Photovoltaics: The Search for New Materials. *Philos. Trans. R. Soc., A* **2011**, *369*, 1840−1856.

(5) Ganose, A. M.; Savory, C. N.; Scanlon, D. O. Beyond Methylammonium Lead Iodide: Prospects for the Emergent Field of Ns^2 Containing Solar Absorbers. *Chem. Commun.* **2017**, *53*, 20−44.

(6) Brandt, R. E.; Stevanović, V.; Ginley, D. S.; Buonassisi, T. Identifying Defect-Tolerant Semiconductors with High Minority-Carrier Lifetimes: Beyond Hybrid Lead Halide Perovskites. *MRS Commun.* **2015**, *5*, 265−275.

(7) Snaith, H. J. Present Status and Future Prospects of Perovskite Photovoltaics. *Nat. Mater.* **2018**, *17*, 372−376.

(8) Wallace, S. K.; Mitzi, D. B.; Walsh, A. The Steady Rise of Kesterite Solar Cells. *ACS Energy Lett.* **2017**, *2*, 776−779.

(9) Tiwari, D.; Skidchenko, E.; Bowers, J.; Yakushev, M. V.; Martin, R.; Fermin, D. J. Spectroscopic and Electrical Signatures of Acceptor States in Solution-Processed $Cu_2ZnSn(S,Se)_4$ Solar Cells. *J. Mater. Chem. C* **2017**, *5*, 12720−12727.

(10) Bourdais, S.; Chone, C.; Delatouche, B.; Jacob, A.; Larramona, G.; Moisan, C.; Lafond, A.; Donatini, F.; Rey, G.; Siebentritt, S.; et al. Is the Cu/Zn Disorder the Main Culprit for the Voltage Deficit in Kesterite Solar Cells? *Adv. Energy Mater.* **2016**, *6*, 1502276−1−21.

(11) Lee, L. C.; Huq, T. N.; MacManus-Driscoll, J. L.; Hoye, R. L. Z. Research Update: Bismuth-Based Perovskite-Inspired Photovoltaic Materials. *APL Mater.* **2018**, *6*, 084502−1−16.

(12) Cao, Y.; Bernechea, M.; Maclachlan, A.; Zardetto, V.; Creatore, M.; Haque, S. A.; Konstantatos, G. Solution Processed Bismuth Sulfide Nanowire Array Core/Silver Sulfide Shell Solar Cells. *Chem. Mater.* **2015**, *27*, 3700−3706.

(13) Hahn, N. T.; Self, J. L.; Mullins, C. B. BiSI Micro-Rod Thin Films: Efficient Solar Absorber Electrodes? *J. Phys. Chem. Lett.* **2012**, *3*, 1571−1576.

(14) Bernechea, M.; Miller, N. C.; Xercavins, G.; So, D.; Stavrinadis, A.; Konstantatos, G. Solution-Processed Solar Cells Based on Environmentally Friendly $AgBiS_2$ Nanocrystals. *Nat. Photonics* **2016**, *10*, 521−525.

(15) Park, B. W.; Philippe, B.; Zhang, X.; Rensmo, H.; Boschloo, G.; Johansson, E. M. J. Bismuth Based Hybrid Perovskites $A_3Bi_2I_9$ (A: Methylammonium or Cesium) for Solar Cell Application. *Adv. Mater.* **2015**, *27*, 6806−6813.

(16) Lehner, A. J.; Wang, H.; Fabini, D. H.; Liman, C. D.; Hébert, C.-A.; Perry, E. E.; Wang, M.; Bazan, G. C.; Chabinyc, M. L.; Seshadri, R. Electronic Structure and Photovoltaic Application of BiI_3. *Appl. Phys. Lett.* **2015**, *107*, 131109−1−4.

(17) Hamdeh, U. H.; Nelson, R. D.; Ryan, B. J.; Bhattacharjee, U.; Petrich, J. W.; Panthani, M. G. Solution-Processed BiI_3 Thin Films for Photovoltaic Applications: Improved Carrier Collection via Solvent Annealing. *Chem. Mater.* **2016**, *28*, 6567−6574.

(18) Tiwari, D.; Fermin, D. J.; Chaudhuri, T. K.; Ray, A. Solution Processed Bismuth Ferrite Thin Films for All-Oxide Solar Photovoltaics. *J. Phys. Chem. C* **2015**, *119*, 5872−5877.

(19) Hoye, R. L. Z.; Lee, L. C.; Kurchin, R. C.; Huq, T. N.; Zhang, K. H. L.; Sponseller, M.; Nienhaus, L.; Brandt, R. E.; Jean, J.; Polizzotti, J. A.; et al. Strongly Enhanced Photovoltaic Performance and Defect Physics of Air-Stable Bismuth Oxyiodide (BiOI). *Adv. Mater.* **2017**, *29*, 1702176−1−10.

(20) Brandt, R. E.; Kurchin, R. C.; Hoye, R. L. Z.; Poindexter, J. R.; Wilson, M. W. B.; Sulekar, S.; Lenahan, F.; Yen, P. X. T.; Stevanovic, V.; Nino, J. C.; et al. Investigation of Bismuth Triiodide (BiI_3) for Photovoltaic Applications. *J. Phys. Chem. Lett.* **2015**, *6*, 4297−4302.

(21) Watanabe, K.; Karasawa, T.; Komatsu, T.; Kaifu, Y. Optical Properties of Extrinsic Two-Dimensional Excitons in BiI_3 Single Crystals. *J. Phys. Soc. Jpn.* **1986**, *55*, 897−907.

(22) Podraza, N. J.; Qiu, W.; Hinojosa, B. B.; Motyka, M. A.; Phillpot, S. R.; Baciak, J. E.; Trolier-Mckinstry, S.; Nino, J. C. Band Gap and Structure of Single Crystal BiI_3: Resolving Discrepancies in Literature. *J. Appl. Phys.* **2013**, *114*, 033110.

(23) Jellison, G. E.; Ramey, J. O.; Boatner, L. A. Optical Functions of BiI_3 as Measured by Generalized Ellipsometry. *Phys. Rev. B: Condens. Matter Mater. Phys.* **1999**, *59*, 9718−9721.

(24) Dmitriyev, Y. N.; Bennett, P. R.; Cirignano, L. J.; Klugerman, M. B.; Shah, K. S. Bismuth Iodide Crystals as a Detector Material: Some Optical and Electrical Properties. *Proc. SPIE* **1999**, *3768*, 521−529.

(25) Lintereur, A. T.; Qiu, W.; Nino, J. C.; Baciak, J. Characterization of Bismuth Tri-Iodide Single Crystals for Wide Band-Gap Semiconductor Radiation Detectors. *Nucl. Instrum. Methods Phys. Res., Sect. A* **2011**, *652*, 166−169.

(26) Tiwari, D.; Fermin, D. J. Textured PbI_2 Photocathodes Obtained by Gas Phase Anion Replacement. Electrochim. *Electrochim. Acta* **2017**, *254*, 223−229.

(27) Drago, R. S. On Pearson's Quantitative Statement of HSAB. *Inorg. Chem.* **1973**, *12*, 2211−2212.

(28) Zobel, J.; Trotter, T. The Crystal Structure of SbI_3 and BiI_3. *Zeitschrift für Krist.* **1966**, *123*, 67−72.

(29) Sun, X. X.; Li, Y. L.; Zhong, G. H.; Lü, H. P.; Zeng, Z. The Structural, Elastic and Electronic Properties of BiI_3: First-Principles Calculations. *Phys. B* **2012**, *407*, 735−739.

(30) Schluter, M.; Cohen, M. L.; Kohn, E.; Fong, Y. Electronic Structure of BiI_3. *Phys. Status Solidi B* **1976**, *78*, 737−747.

(31) Yorikawa, H.; Muramatsu, S. Theoretical Study of Crystal and Electronic Structures of BiI_3. *J. Phys.: Condens. Matter* **2008**, *20*, 325220−1−7.

(32) Kaifu, Y.; Komatsu, T. Optical Properties of Bismuth Tri-Iodide Single Crystals. II. Intrinsic Absorption Edge. *J. Phys. Soc. Jpn.* **1976**, *40*, 1377−1382.

(33) Zhang, W.-B.; Xiang, L.-J.; Li, H.-B. Theoretical Perspective of Energy Harvesting Properties of Atomically Thin BiI_3. *J. Mater. Chem. A* **2016**, *4*, 19086−19094.

(34) Komatsu, T.; Kaifu, Y. Optical Properties of Bismuth Tri-Iodide Single Crystals. I Interband Transitions. *J. Phys. Soc. Jpn.* **1976**, *40*, 1062−1068.

(35) Van Schilfgaarde, M.; Kotani, T.; Faleev, S. Quasiparticle Self-Consistent GW Theory. *Phys. Rev. Lett.* **2006**, *96*, 226402.

(36) Hautier, G.; Miglio, A.; Ceder, G.; Rignanese, G. M.; Gonze, X. Identification and Design Principles of Low Hole Effective Mass P-Type Transparent Conducting Oxides. *Nat. Commun.* **2013**, *4*, 2292.

(37) Du, M. H.; Singh, D. J. Enhanced Born Charges in III-VII, IV-VII_2, and V-VII_3 Compounds. *Phys. Rev. B: Condens. Matter Mater. Phys.* **2010**, *82*, 045203.

(38) Ganose, A. M.; Butler, K. T.; Walsh, A.; Scanlon, D. O. Relativistic Electronic Structure and Band Alignment of BiSI and BiSeI: Candidate Photovoltaic Materials. *J. Mater. Chem. A* **2016**, *4*, 2060−2068.

(39) Repins, I. L.; Metzger, W. K.; Perkins, C. L.; Li, J. V.; Contreras, M. A. Correlation between Measured Minority-Carrier Lifetime and $Cu(In,Ga)Se_2$ device Performance. *IEEE Trans. Electron Devices* **2010**, *57*, 2957−2963.